Taylor & Francis
Taylor & Francis Group

Inhalation Toxicology

International Forum for Respiratory Research

ISSN: 0895-8378 (Print) 1091-7691 (Online) Journal homepage: https://www.tandfonline.com/loi/iiht20

Positron emission tomography: A novel technique for investigating the biodistribution and transport of nanoparticles

Heather A. Palko, Jennifer Y. Fung & Angelique Y. Louie

To cite this article: Heather A. Palko, Jennifer Y. Fung & Angelique Y. Louie (2010) Positron emission tomography: A novel technique for investigating the biodistribution and transport of nanoparticles, Inhalation Toxicology, 22:8, 657-688, DOI: 10.3109/08958371003713745

To link to this article: https://doi.org/10.3109/08958371003713745

Inhalation Toxicology, 2010; 22(8): 657–668

informa
healthcare

RESEARCH ARTICLE

Positron emission tomography: A novel technique for investigating the biodistribution and transport of nanoparticles

Heather A. Palko[1], Jennifer Y. Fung[2], and Angelique Y. Louie[2]

Departments of [1]Chemistry and [2]Biomedical Engineering, University of California–Davis, Davis, California, USA

Abstract

Particulate matter (PM) has been associated with serious health effects within but also outside of the pulmonary system. Therefore, there is great interest in studying the biodistribution of PM after delivery to the lung to correlate sites of extrapulmonary particle accumulation and abnormal conditions known to be associated with PM exposure. Traditional PM tracking studies have introduced nanoparticles to animal models or humans and have determined the biodistribution with gamma counting, gamma camera, and inductively coupled plasma mass spectrometry (ICP-MS). The authors here demonstrate that positron emission tomography (PET) is a powerful tool that can be employed to visualize the deposition and track the fate of nanoparticles in the mouse model. In these studies, ~100-nm polystyrene nanoparticles were labeled with the positron emitter ^{64}Cu bound by the chelator (*S*)-2-(4-isothiocyanatobenzyl)-1,4,7,10-tetraazacyclododecane-tetraacetic acid (*p*-SCN-Bn-DOTA). The labeled nanoparticles were instilled intratracheally into C57BL/6 mice; the initial deposition and biodistribution through 48 h was determined by PET imaging. In addition to static imaging, dynamic imaging was performed in the Sprague-Dawley rat model to demonstrate that PET can capture particle movement in pseudo-time-lapse videos. Particle deposition and clearance was clearly identified by PET, and the same animals could be imaged repeatedly without any adverse effects from anesthesia. PET has the potential to require many fewer animals than traditional methods while still providing quantitative results. In addition, the initial deposition pattern in each animal can be accurately determined and the same animal monitored over time so that data interpretation is not clouded by variations in initial deposition profiles.

Keywords: *Biodistribution; nanoparticles; particulate matter; positron emission tomography*

Introduction

Air pollution of all types is likely to affect human health and has been linked to impaired lung function and lung diseases, including lung cancer (Brunekreef and Holgate, 2002). It recently has been shown that there is a probable correlation between exposure to particulate matter (PM) air pollutants and morbidity (Ostro, 1990; Peters et al., 1997) and mortality (Dominici et al., 2003; Laden et al., 2000; Laden et al., 2006; Reich et al., 2009; Stölzel et al., 2006). Health effects are experienced not only in the respiratory system but also throughout the body, including the cardiovascular system (Gerlofs-Nijland et al., 2005; Riediker et al., 2004; Wichers et al., 2004). For example, epidemiological studies have observed that the risk of myocardial infarction (MI) increases significantly after acute exposures. Peters et al. found an increased risk for MI in individuals 2 h after exposure to elevated concentrations of fine particles (≤2.5 μm) (Peters et al., 2001), and also observed an increased risk to onset of MI within 1 h postexposure to traffic (Peters et al., 2004). In chronic exposure studies, exposure to particles has been correlated with increased risk of cardiovascular disease and mortality in people 65 and older using regression models (Saldiva et al., 1995; Schwartz et al., 1995). Saldiva et al. found over a 1-year period that an increase of PM_{10} (100 μg/m^3) was associated with a 13% increase in overall mortality in Sao Paulo, Brazil (Saldiva et al., 1995). Over the course of 3 years, Schwartz et al. found an association between PM_{10} and daily admissions for ischemic heart disease in Detroit, Michigan (Schwartz et al., 1995).

The mechanism for how inhaled particles can generate these extrapulmonary effects is still unclear. Are

Address for Correspondence: Angelique Y. Louie, Department of Biomedical Engineering, One Shields Avenue, University of California–Davis, Davis, CA 95616, USA. E-mail: aylouie@ucdavis.edu

(Received 22 May 2009; revised 05 January 2010; accepted 18 February 2010)

ISSN 0895-8378 print/ISSN 1091-7691 online © 2010 Informa UK Ltd
DOI: 10.3109/08958371003713745

extrapulmonary complications downstream effects of respiratory impairment? Do particles retained in the lung induce systemic effects? Can particles travel out of the lungs into circulation to directly affect peripheral organs? Several studies have shown that ultrafine particles (<0.1 μm) have increased toxicity compared with larger particles, on an equal mass basis (Oberdörster et al., 1990, 1994). In addition, it has been shown that ultrafine particles are more proatherogenic (Araujo et al., 2008) and can increase inflammation compared to fine PM (Donaldson et al., 2000). Much effort has been devoted to determining if ultrafine PM deposited into the lungs travels to other organs (Oberdörster et al., 2002; Yu et al., 2007). Studies in the literature to date have investigated the translocation of nanoparticles in humans and animals using highly sensitive detection methods, including the gamma camera, inductively coupled plasma mass spectrometry (ICP-MS), and gamma counting.

In human PM studies, the transport and retention of nanoparticles is determined by a gamma camera. The gamma camera has an intrinsic spatial resolution of 2.5–4.2 mm, with a sensitivity of $1–1.5\times10^{-4}$ cps/Bq (0.01–0.15%) (Bushberg et al., 2002; Cherry et al., 2003). Studies in the literature commonly use ^{99m}Tc-labeled carbon nanoparticles, which are produced by a commercially available generator equipped with graphite electrodes and pertechnetate solution (Brown et al., 2000). Subjects inhale the nanoparticles, planar (two-dimensional) images are generated, and regions of interest (ROI) can be selected for quantifying particle content (Brown et al., 2002; Nemmar et al., 2002; Wiebert et al., 2006a, 2006b). Small animal gamma cameras are available and have been used in the literature to study mucociliary function and particle accumulation and clearance after chronic exposure to diesel particles, but they are not used extensively for particulate matter tracking studies (Wolff et al., 1987; Foster et al., 2001). Single-photon emission computed tomography (SPECT), a technique that utilizes gamma cameras to obtain three-dimensional information, has also been used in small animals to determine the biodistribution of ^{99m}Tc-labeled fullerenes (Xu et al., 2007). The small animal gamma camera has a spatial resolution of 2–3 mm and sensitivity typically of 1% or less (Loudos et al., 2003; Franc et al., 2008). Gamma cameras are capable of determining the initial deposition pattern in the lungs and translocation to other organs; however, unless SPECT is utilized, they do not provide three-dimensional information.

In animal models, studies typically involve introducing the particles to the lungs and then determining their biodistribution over time by assaying extracted organs ex vivo (Kreyling et al., 2002; Nemmar et al., 2001; Oberdörster et al., 2002; Takenaka et al., 2006). These studies commonly use gamma counting and ICP-MS as detection methods. In gamma counting studies, radiolabeled particles are generated with spark and spinning disk generators. These particle generation methods incorporate the radiolabel (^{192}Ir, ^{57}Co) while synthesizing the particles (Kreyling et al., 1993, 2002; Semmler et al., 2004). The gamma counter is highly suitable for measuring small quantities of activity (<37 Bq); the instrument exhibits high detection efficiency for most γ-ray emitters (Cherry et al., 2003; Bushberg et al., 2002). Although this technique is attractive because of its detection capabilities, it cannot provide information on initial lung deposition in each animal or particle distribution within each organ and it requires numerous animals for each time point of interest to control for animal variations.

ICP-MS is another ex vivo technique that is utilized to determine biodistribution of particles. Particles for these studies are commonly produced by a spark generator and are comprised of metals or nonmetals (i.e., carbon, silver, gold) (Oberdörster et al., 2002, 2004; Takenaka et al., 2001, 2006). These particles are easily detected by ICP-MS due to its high sensitivity (ppb) and multielement and isotope capabilities (Ding et al., 1999). Biological samples for this technique require sample preparation before analysis; this is accomplished with homogenization or digestion of the tissue (Oberdörster et al., 2004; Takenaka et al., 2001). Although this technique is used because of its superior trace level analysis, it also does not provide information on particle distribution within the tissue or initial lung deposition and requires a large number of animals per time point for statistical relevance.

Although the above-referenced methods have been used extensively, each method lacks some critical element to fully characterize particle transport. Other methods of detection could yield more information than these methods can provide. In this work we evaluate positron emission tomography as a method for tracking particle fate in animal models.

Positron emission tomography (PET) is a noninvasive, nuclear imaging technique that is capable of visualizing deep tissues with a high sensitivity of 0.02–0.10 cps/Bq (2–10%). PET instrumentation is available for both humans and small animals, with a spatial resolution of 4 mm and 1–1.8 mm, respectively. Positron-emitting radionuclides, such as ^{11}C, ^{64}Cu, and ^{18}F, are used to label a compound of interest and track its biodistribution. Once a positron is emitted from the nucleus of a radionuclide, it can annihilate with a nearby electron in the tissue, resulting in the emission of two gamma rays (511 keV) 180° apart. These gamma rays can then be detected and localized in space, forming a "coincidence" event. The collection of events can then be used to identify the location of the positron-emitting isotope in a volume (Cherry, 2001; Wilson, 1998). With PET one can generate a three-dimensional image or map of processes in living subjects (Tai et al., 2003). Mathematical reconstruction methods and correction factors are then used to generate cross-sectional images through the object, which can be analyzed quantitatively using regions of interest (ROI) to determine the concentration of isotope in a region (Cherry et al., 2003; Wilson, 1998).

PET could be a powerful tool for studying the fate of nanoparticles delivered to the lung. PET is capable of visualizing the initial deposition in the lungs, identifying distribution within secondary organs and tracking the same animal over time. Knowledge of the initial deposition pattern is critical for interpretation of data of later time points, as within the respiratory system clearance mechanisms differ by region (McClellan and Henderson, 1989). In addition, tracheal

versus esophageal delivery of particles involve markedly different clearance mechanisms and it can be difficult to interpret transport data unless initial deposition strictly to the respiratory tract is confirmed. Although gamma cameras can provide two-dimensional deposition and secondary organ distribution information, this technique is less sensitive than PET and has a lower resolution for small animal systems (Table 1).

In this work, we radiolabel 100-nm nanoparticles with ^{64}Cu (half life = 12.7 h) for instillation into the lungs of mice. We investigate the utility of PET for studying transport of nanoparticles from the lung and assess its capabilities. The nanoparticles synthesized serve as a model system of similar size to ultrafine particles.

Materials and methods

Chemicals for polystyrene nanoparticle labeling

Surfactant-free aliphatic amine polystyrene nanoparticles, 2.0% *w/v* (Molecular Probes, Invitrogen, Eugene, OR), (*S*)-2-(4-isothiocyanatobenzyl)-1,4,7,10-tetraazacyclododecane-1,4,7,10-tetraacetic acid (*p*-SCN-Bn-DOTA; Macrocyclics, Dallas, TX), acetic acid, glacial (EM Science, Gibbstown, NJ), triethanolamine (>99%; Fluka, (Buchs, Switzerland)), and cupric-64 chloride solution (half life = 12.7 h) (MDS Nordion, Ottawa, Canada, and Trace Life Sciences, Denton, TX) were used as purchased. Specific activities for the cupric-64 chloride solution for MDS Nordion and Trace Life Sciences were 1.41×10^{17} and 4.1×10^{15} Bq/g, respectively.

Polystyrene nanoparticle labeling

The copper metal for this radiolabeling was preinserted into the chelator (Jarrett et al., 2008). This preinsertion method was also followed by Moi et al. in which a TETA (1,4,8,11-tetraazacyclotetradecane-*N*,*N*′,*N*″,*N*‴-tetraacetic acid) analog was used as the macrocyclic chelating agent (Moi et al., 1985). $^{64}CuCl_2$ (74 MBq, approximately 0.6 nmol, in 200 µl of 10 mM HCl) was buffered with 0.1 M triethylammonium acetate (TEAA) buffer (pH 8, 30 µl) and added to *p*-SCN-Bn-DOTA (0.14 µmol in 10 µl), then incubated at 41°C for 20 min. To a polystyrene nanoparticle solution (1.68 mg in 800 µl water) 0.1 M TEAA was added to adjust the solution to pH 8 (80 µl). The polystyrene nanoparticle solution was added to the reaction mixture and this solution was incubated at 53°C for 2 h. The nanoparticles were then centrifuged at 4000 rpm for 15 min, the supernatant was removed, and the nanoparticles were resuspended in saline (600 µl). This purification process was repeated two additional times. The labeled nanoparticles in saline were passed through a sterile 0.22-micron filter prior to instillation. Transmission electron microscopy (TEM) (Phillips CM-120) operating at 80 keV was used to visualize the particle size before and after labeling. Nanoparticle size was determined with Image J, a Java-based image processing program.

Table 1. Summary of PM transport detection methods.

Detection	Resolution	Sensitivity	Initial deposition?
Gamma counting	N/A	≤1 nCi	No
ICP-MS	N/A	ppb	No
Gamma camera			
Human	2.5–4.2 mm	0.01–0.15%	Yes (2D)
Small animal	2.0–3.0 mm	≤1%	Yes (2D)
PET			
Human	4.0 mm	2–10%	Yes (3D)
Small animal	1–1.8 mm	2–10%	Yes (3D)

Animals and instillation delivery

All animal experiments were conducted under a protocol approved by the University of California, Davis, Animal Use and Care Committee (Davis, CA). Male and female C57BL/6 mice, 15–27 g, and a male Sprague-Dawley rat, 80 g (Charles River, Wilmington, MA) were housed in a temperature controlled (22°C) room in ventilated cages. All animals were maintained on a 12-h day/night cycle prior to studies. Animal diet and water were provided ad libitum. Animals were anesthetized with isoflurane (2–3.0%) prior to instillation. Nanoparticles were delivered using a Hamilton flat-tipped syringe (40 µl) intratracheally or directly into the esophagus at concentrations of 1.2×10^{14} nanoparticles/ml to mice for lung ($n = 4$), dynamic intravenous ($n = 4$), or gavage ($n = 3$); and at 1.25×10^{14} nanoparticles/ml to the rat ($n = 1$) for the dynamic lung instillation. The instilled dose delivered to the animal was determined by measuring the amount of radioactivity in the delivery syringe before and after the instillation with a dose calibrator; the difference was used as the initial, or instilled dose (ID). Nanoparticle accumulation data from all later time points were referenced against this ID. As a control, $^{64}CuCl_2$ (1 ng $CuCl_2$) was delivered to the lungs of mice ($n = 5$) as previously stated for the nanoparticles (Hamilton Company, Reno, NV). This dose was comparable to the labeled particles (1.5 ng ^{64}Cu/dose).

Imaging and gamma counting

PET images were obtained on a microPET-Focus 120 (Siemens Medical Solutions, Malvern, PA). The Focus 120 has a transaxial field of view of 10 cm and an axial field of view of 7.6 cm, with a spatial resolution of 1.3 mm. The circular detector array consists of 96 detector blocks with a face-to-face diameter of 15 cm (Kim et al., 2007). The animals were followed for up to 48 h using ^{64}Cu as the radioisotope (12.7 h half life). For all PET scans, animals are anesthetized with a 1.5% isoflurane maintenance dose for static scans that were 15 min for the 0-, 2-, 4-, and 12-h time points, and 1 h in duration for the 24- and 48-h time points. Images were reconstructed using a maximum a posteriori algorithm (MAP). Static scans yield a single image that represents the average intensities for a given acquisition time.

Dynamic scans were taken as a 1-h static scan and reconstructed into frames using a maximum a posteriori algorithm (MAP). For the dynamic scans, the acquisition protocol was the same, but during postacquisition processing images were reconstructed in specified "frames" that span the acquisition time—this allows us to generate short movies that can show the change in signal intensity and distribution of particles

over the acquisition period. For each frame of a dynamic scan, the counts were averaged for the length of time of the frame. Protocols for the following dynamic scans were chosen in order to illustrate movement of nanoparticles during the length of the scan. These protocols were unique for each type of delivery (instillation, intraveneous). A 27-frame protocol was used to visualize the instillation of nanoparticles into the lungs of a rat during the 1-h scan (illustrated below). The 27-frame reconstruction can be illustrated as shown in Scheme 1. Shorter time periods were averaged in the earlier time frames where more particle movement was expected to occur. In this case the instillation was expected to show more particle movement; this point in time is indicated in the series by a red arrow. For the intraveneous dynamic scan, a 26-frame protocol was used and was segmented as follows: frames 1–10 (1 s each) + frames 11–15 (10 s each) + frames 16–19 (60 s each) + frames 20–22 (3 sec each) + frames 23–26 (600 s each). Earlier frames averaged shorter time periods for this dynamic scan in order to show the nanoparticle injection and systemic distribution before localizing in one area.

In the current studies, respiratory gating was not performed, as the breathing of the animals was shallow and slow enough not to cause significant blurring of the images. If an application requires it, respiratory gating can be used to correct any blurring from motion. In respiratory gating, signal acquisitions are triggered to occur at the same point in the respiratory cycle; this ensures that the lung tissue is in the same position for each scan. The degree of motion of the lung in the mouse model appears to be smaller than the resolution limit; thus, in general, respiratory gating does not affect image quality (Yang et al., 2005) and is not commonly used for quantitative PET studies (Doot et al., 2007 and Rossin et al., 2008).

A small animal micro–computed tomography (CT) scanner equipped with a variable focus low-power x-ray tube source (microCAT II; Siemens, Knoxville, TN) was used to obtain anatomical data to correlate with PET distribution. For the acquisition, the scanner was in standard resolution mode with a 0.5-mm aluminum filter. Data were reconstructed with the reconstruction, visualization, and analysis (RVA) software package with the high-speed COne Beam Reconstruction Algorithm (COBRA) option using a Feldkamp reconstruction algorithm and Shepp-Logan filter type. The image matrix was $2048 \times 2048 \times 3072$ pixels and the corresponding voxel size was $0.0971\,\text{mm} \times 0.0971\,\text{mm} \times 0.0971\,\text{mm}$. CT and PET images were overlayed by using external fiducial markers. Fiducial markers are positive contrast, fixed points of reference. The fiducial markers were correlated between the data sets by using the Fusion tool in the ASIPro Virtual Machine software. The fusion tool allows the user to align the fiducial markers for overlay in the *X*, *Y*, and *Z* direction.

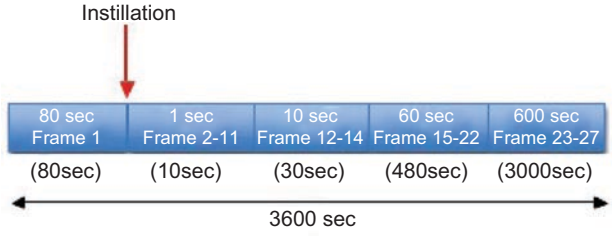

Scheme 1. Dynamic protocol for the instillation of nanoparticles.

Using the PET images, tissue radioactivity was quantified by defining regions of interest (ROI) and calculating the total radioactivity in these regions using the total activity value given by the ASIPro Virtual Machine software. ROI were assigned by the observer based on increased signal intensity versus background, and were drawn by hand using the ROI tool in the software. All values for ROI were decay corrected to the 0-h time point for comparison. Percent injected dose (%ID) is determined by dividing the corrected ROI value for a given organ by the instilled dose and multiplying by 100. Deposited dose (DD) is calculated by dividing the total activity in the lungs at time 0 by the instilled dose (ID). Lung retention is given by the activity remaining at 48 h relative to DD.

A Wallac Wizard Automatic Gamma Counter Model 1470 (Perkin Elmer, Waltham, MA) was used for the detection limit measurements. A Fluke Biomedical Dose calibrator (34-162 CAL/RAD MARK IV, Cleveland, OH) was used to calculate doses of labeled nanoparticles delivered to each animal, as well as for in vitro stability measurements, and for excreta and carcass measurements.

Limit of detection of polystyrene nanoparticles

Labeled nanoparticles were prepared as described above. A series of dilutions of the nanoparticles were imaged using PET for 30 min on a 96-well plate. Images were reconstructed using a maximum a posteriori algorithm (MAP). For all solutions (nanoparticles/ml) 100 µl and 200 µl of each concentration was imaged to determine volume effects. After imaging, all samples were gamma counted for comparison.

Stability of 100-nm particles

^{64}Cu-labeled polystyrene nanoparticles were incubated in three different solutions to assess stability of the complexed copper in saline, saline at pH 2, and plasma. Particles were incubated with each solution for up to 48 h. An aliquot (30 µl) was taken at each time point (0, 1, 2, 4, 24, and 48 h) and measured for initial activity (before purification) using a dose calibrator. Each aliquot was centrifuged in filtered tubes from Millipore (Billerica, MA; molecular weight cutoff [MWCO] = 3000) at 14,500 rpm for 15 min to separate dissociated copper in solution from labeled nanoparticles on the filter. Final activity (post purification) was taken for the nanoparticles on the filter. Comparisons between values were made using least squares means *t* test. Differences between values were considered significant when $p < .01$.

Results

Particle characterization

Unlabeled and labeled nanoparticles did not show a significant change in size after labeling as determined by TEM. The average size for both the unlabeled and labeled nanoparticles was 101 ± 7.6 nm and 103 ± 10.9 nm, respectively. Figure 1 shows a representative TEM image of the labeled nanoparticles.

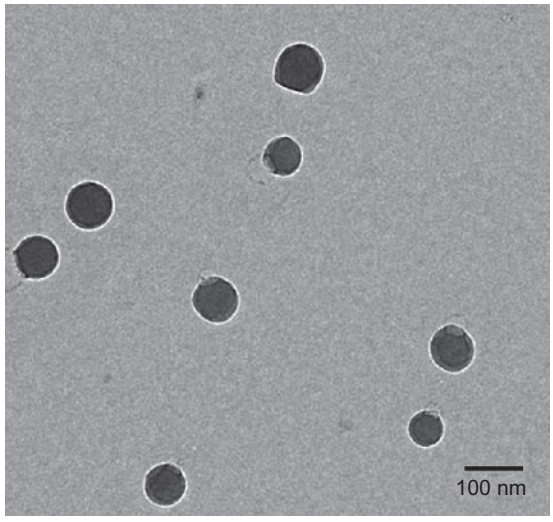

Figure 1. TEM of labeled nanoparticles. Mean diameter is 103 ± 10.9 nm.

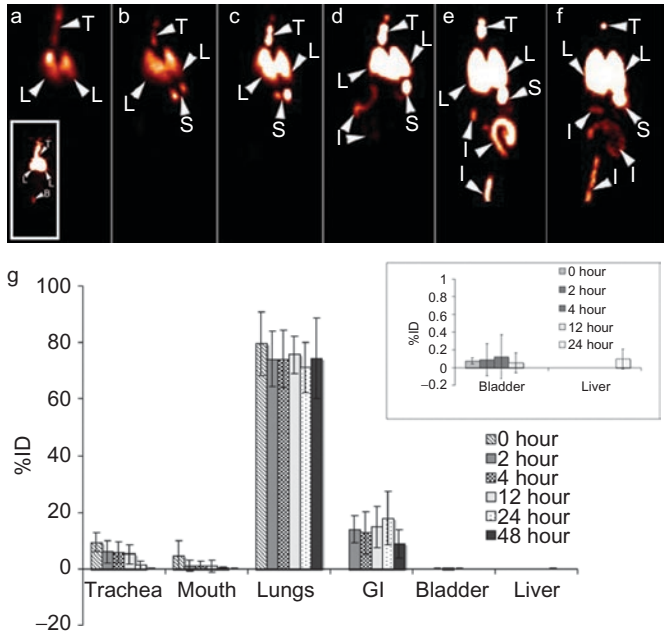

Figure 2. Clearance of nanoparticles from the lungs of the mouse at (a) 0, (b) 2, (c) 4, (d) 12, (e) 24, and (f) 48 h. Nanoparticles are present in T = trachea, L = lungs, S = stomach, and I = intestines. A single slice from the volume in (a) shows bladder signal B = bladder (see inset). Biodistribution over 48 h in (g) shows particles in the trachea, gastrointestinal tract (GI), and liver ($n = 4$). Inset shows rescaled bladder and liver signal over 48 h.

PET is able to visualize particle deposition to the lungs and transport over time

Figure 2 shows representative PET images for up to 48 h after nanoparticle instillation into the lungs in the mouse model. For all of the animals in this work, the instilled dose was distributed evenly to both lungs. In this, image and all other images shown, the signal is presented as a three-dimensional (3D) projection in the ventral-dorsal orientation unless otherwise noted. Figure 2a shows initial deposition into the trachea and lungs; Figure 2b–f show biodistribution patterns over 48 h, revealing nanoparticles in the trachea, lungs, stomach, and intestines. A single slice from the 0-h scan is shown in the inset to illustrate signal intensity in the bladder.

PET is both a qualitative and a quantitative imaging method and the amount of activity in each organ over time can be calculated using ROI (regions of interest). Biodistribution over 48 h is shown quantitatively in Figure 2g ($n = 4$). Over time, nanoparticles move out of the mouth and trachea via mucociliary clearance and through the gastrointestinal (GI) tract, as shown by the decrease of signal over time in both the mouth and trachea and the increase of signal in the GI tract beginning at 2 h. Nanoparticles in small amounts are also found in the bladder and liver (see inset); bladder signal is present within the first 15 min after instillation (0 h) through the 12-h time point and liver signal is shown only at the 24-h time point. There is no significant loss of signal from the lungs, indicating that negligible amounts of nanoparticles translocated out of the lungs; this is shown by the steady signal for the lungs over 48 h. The amount retained in the lungs at 48 h corresponds to 93.89% ±13.83% of the deposited fraction (Table 2); the rate of loss from the lungs is –0.54%DD/h, where DD = deposited dose. After the 48-h time point, signal in the carcass and excreta were measured by a dose calibrator, these accounted for the remaining dose ($n = 2$).

Biodistribution over time after stomach deposition, gavage, was very different compared to that described above for lung deposition. Figure 3a shows an example of a gavage of polystyrene nanoparticles into the esophagus and stomach. Clearance of nanoparticles from the esophagus to the GI tract is shown over 48 h in Figure 3b–e ($n = 3$). The rate of loss of nanoparticles from the esophagus is –30.16%DD/h. This rate differs considerably from the rate of loss of particles from the lungs (–0.54%DD/h). Figure 3f shows quantification of signal over time. Over 48 h nanoparticles clear from the mouth and esophagus into the GI tract and nearly all of the particles have cleared from the GI tract by 48 h.

Free copper clearance differs from that of particles

To ensure that the signal in the images is from polystyrene nanoparticles and not free dissociated copper, the clearance of free instilled copper was studied with PET. Figure 4 shows clearance of free copper over 48 h in the mouse ($n = 5$). Figure 4a confirms instillation into the trachea and lungs and Figure 4b–e show the biodistribution of free copper over 48 h. The biodistribution over 48 h is quantified in Figure 4f. Over 48 h free copper is cleared from the mouth, trachea, and lungs; this is shown by the decrease in signal for these organs over time. Free copper leaves the lungs in an exponential fashion ($y = 70.762e^{-0.0337x}$; $R^2 = .97$) with only 18.52% ± 4.50% of the deposited fraction remaining after 48 h (Table 2). This rate of clearance for free copper (average –4.10%DD/h, 16 h half-time) differs from the rate of nanoparticle clearance (–0.54%DD/h). Note that a half-time for particles could not be calculated due to the slow rate of clearance. Secondary organ transport also differs from nanoparticle transport. Free copper accumulates in the liver over time, whereas particles did not. As shown in the inset, small amounts of free copper are present in the kidneys and bladder.

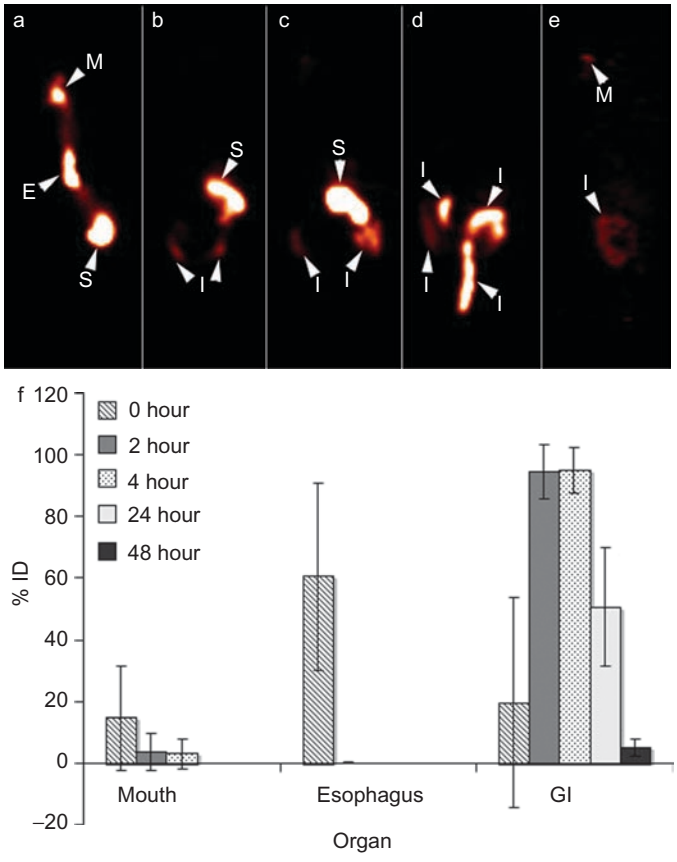

Figure 3. Clearance of nanoparticles from the stomach into the intestines in the mouse at (a) 0, (b) 2, (c) 4, (d) 24, and (e) 48 h. Nanoparticles are present in M = mouth, E =esophagus, S = stomach, and I = intestines. (f) Biodistribution over 48 h shows that nanoparticles clear from the mouth and esophagus through the GI tract ($n = 3$).

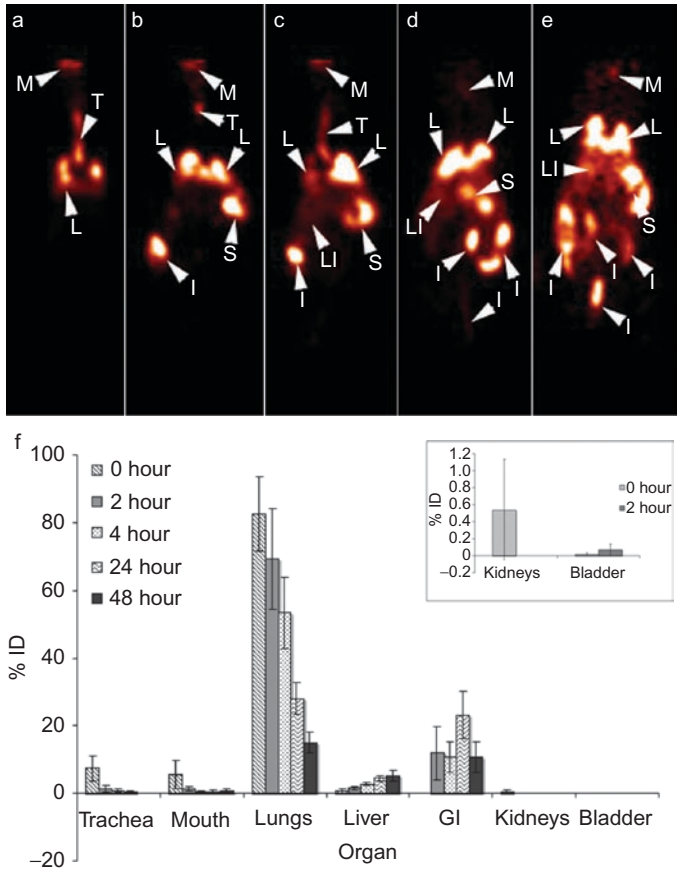

Figure 4. Clearance of free copper in the mouse at (a) 0, (b) 2, (c) 4, (d) 24, and (e) 48 h. Free copper is shown in the M = mouth, T = trachea, L = lungs, S = stomach, I = intestines, and LI = liver. (f) Biodistribution through 48 h is found in the liver, stomach, and gastrointestinal tract (GI) ($n = 5$). Inset shows rescaled kidney and bladder signal over 48 h.

Dynamic imaging allows pseudo-time-lapse tracking of particle movement

Figure 5 displays frames of a dynamic scan using PET during and over the first hour after instillation to a rat model. The rat model was used due to the ease of performing the instillation while the animal was positioned in the imaging system. Figure 5a presents a view primarily of the tracheal region, whereas Figure 5b is centered on the thoracic cavity. (See Supplementary Data, 27-frame movies.) In Movie A, the movement of nanoparticles from the trachea into lungs during instillation is seen. Movement of nanoparticles in the lungs after deposition is shown in Movie B. The particles were primarily deposited to the upper portion of each lung, with the left lung receiving more of the dose. As movie B progresses, movement of nanoparticles through each lobe is shown.

Another example of dynamic imaging is shown in supplemental Movie C. Movie C shows intraveneous transport of the labeled nanoparticles in the mouse. Upon injection via tail vein, the nanoparticles move through the inferior vena cava to the heart. From the heart, the signal (particles) is pumped throughout the body, then gradually concentrates and the carotids and liver begin to appear. Finally, the signal (particles) concentrates in the liver and spleen. (Supplementary Data, 26-frame movie.)

Table 2. Average deposited fraction in the lung (%ID) and lung retention at 48 h.

Label/particle	Deposited fraction ± *SD*	Lung retention ± *SD*
Polystyrene	79.54 ± 11.19	93.89 ± 13.83
Free copper	82.48 ± 10.98	18.52 ± 4.50

Multimodal imaging can provide anatomical reference when needed

In the data shown, identification of organs was straightforward, as the distribution of the PET signal was such that organ boundaries could easily be identified. Overlaying CT anatomical referencing with the PET images can help assign organs that are not as easily identified. In Figure 6, computed tomography (CT) is overlayed with PET to verify lung deposition in the mouse. The CT image allows identification of soft tissue boundaries so that the PET signal position can be correlated to specific organs (I = intestines, L = lungs, S = stomach).

Radiolabeled particles are stable under a variety of conditions

To confirm that the radiolabel remains attached to the nanoparticles and further verify that extrapulmonary distribution

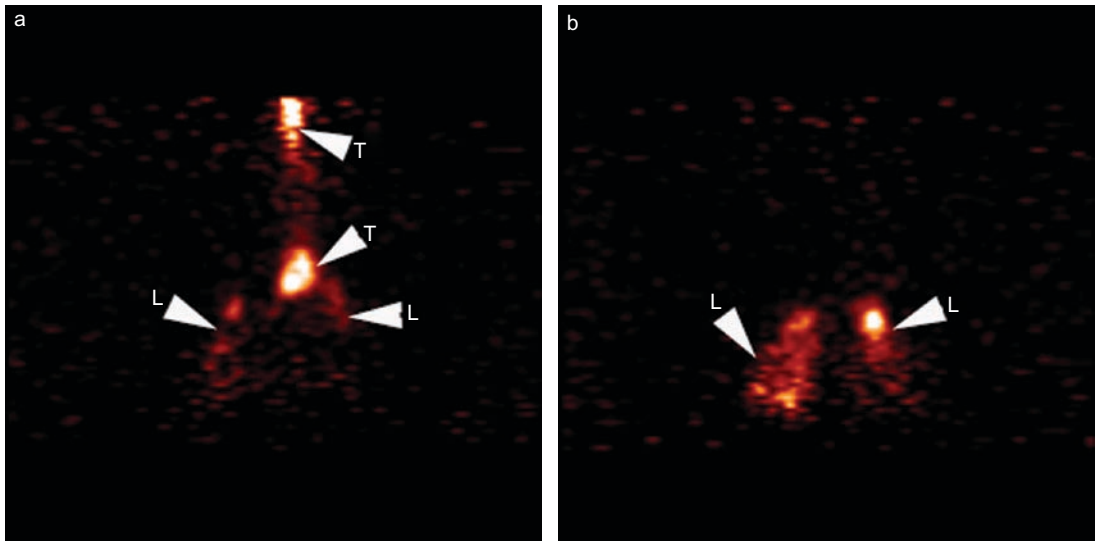

Figure 5. Single frames from dynamic scans of a rat instillation showing (a) trachea and lungs and (b) lungs. Signal found in T = trachea and L = lung. (See supplementary movies.)

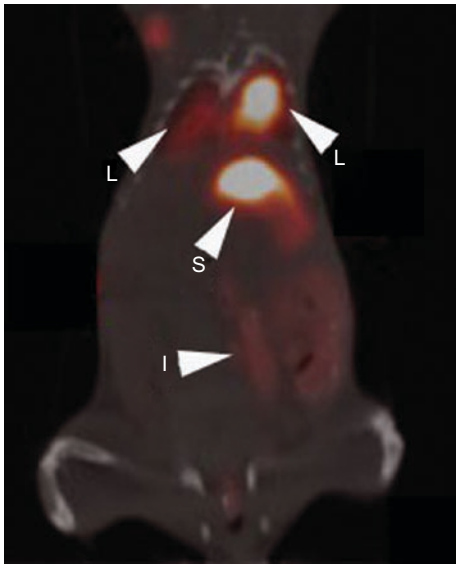

Figure 6. CT overlay with PET showing anatomical details in the mouse. Signal is present in L = lung, S = stomach, and I = intestines.

is not due to free dissociated copper, a stability test was performed to demonstrate that copper remains associated with the nanoparticles over the 48-h time period. Figure 7 shows that over time, the polystyrene nanoparticles in saline, in saline at pH 2, and in plasma do not lose radiolabel. These solutions were prepared to mimic environments that might be encountered in vivo. The saline solution is a control to test the stability of the nanoparticles in solution before instillation. Saline at pH 2 mimics the acidic environment of the stomach and also the lysosomal compartment in cells, representing conditions that may be encountered during GI clearance or ingestion by macrophages. The size of the particles, 100 nm, is at the threshold for triggering uptake by macrophages (Brannon-Peppas and Blanchette, 2004). The plasma solution represents the environment after translocation through the bloodstream. Overall there was no significant loss of copper from the particles under any conditions, confirming the exceptional stability of the chelator.

PET detection limits

The practical detection limit of PET was determined by imaging a series of concentrations of the labeled nanoparticles. Detection limit refers to the lowest concentration of particles that can produce contrast under the given experimental conditions (specific activity of the probe, volume of interest, etc.); this is different than sensitivity, which is a measure of the ability of the detectors to respond to input signal. With decreasing concentration, the intensity of the signal decreased in a linear fashion as expected. Figure 8 plots intensity of the PET image against particle concentration. The lowest detectable concentration was 1.55×10^{10} nanoparticles/ml ($R^2 = .974$) for the degree of radiolabeling used in these studies (4.3×10^{-18} Ci/nanoparticle). Each concentration was detected with gamma counting for comparison, and the limit of detection by gamma counting was 3.87×10^9 nanoparticles/ml.

Discussion

Our results demonstrate that positron emission tomography is able to visualize deposition patterns immediately after tracer instillation in the mouse model. In addition, biodistribution was tracked for each animal and the percent of activity remaining in the lung could be quantified. In these studies, we observe that ~6% of the instilled dose moves out of the lungs over the 48-h observation period; however, this amount was not quantitatively significant. Particles were measured in the stomach and intestines, indicating mucociliary clearance from the upper respiratory tract to the GI tract had occurred. Small quantities were detected in the liver and bladder. These results suggest that the majority of nanoparticles do not transport into circulation. Furthermore, gavage studies showed no indication of nanoparticle absorption into the bloodstream from the GI tract; Figure 3 confirms this observation with

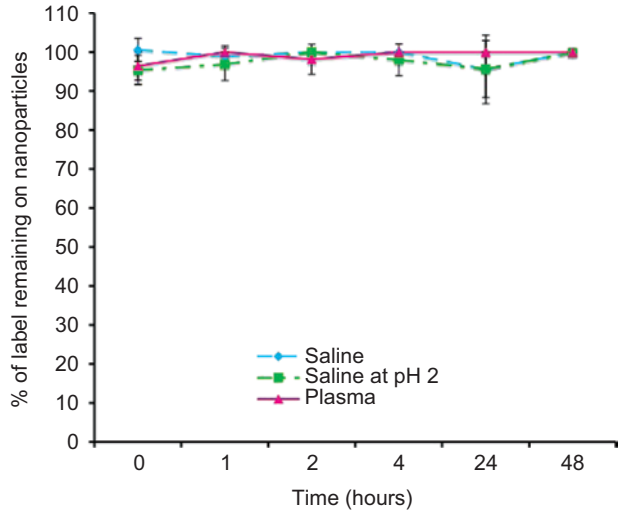

Figure 7. Stability of radiolabeled polystyrene nanoparticles over 48 h in saline, saline at pH 2, and plasma.

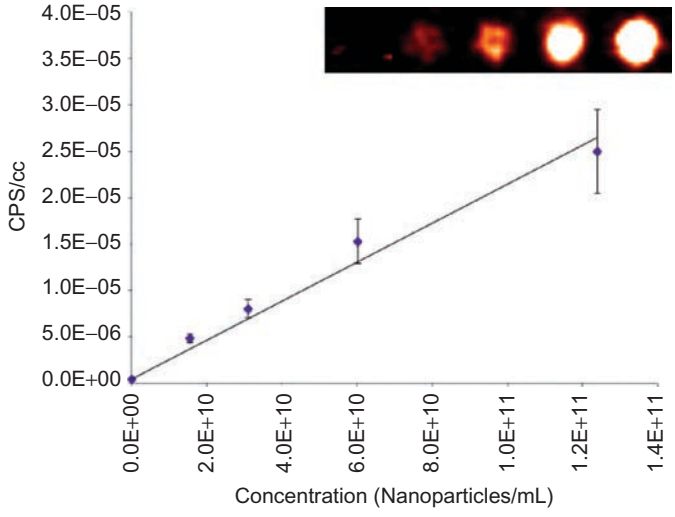

Figure 8. Detection limit for labeled nanoparticles using PET. Intensity in cpm is shown as a function of concentration. Inset shows the actual PET images of the solutions.

nanoparticles clearing solely through the GI tract. Thus, these studies support the conclusion that there is minimal particle clearance to the circulation after instillation.

Table 3 provides an overview of results from transport studies in the literature; the studies most relevant to the work herein are shown with particle sizes in bold. Compared to the literature, our observations are similiar to Wiebert et al. who studied 100nm ^{99m}Tc-carbon particles in humans (Wiebert et al., 2006a). The amount retained in the lungs for Wiebert's study was 99% at both 24 and 48 h, which is similar to our values of 89.86% ± 5.11% and 93.89% ± 13.83%, respectively.

Animal studies in the literature using slightly smaller particles (~80 nm) showed less lung retention than we observed. For example, Kreyling et al. studied ^{192}Ir nanoparticles of 80 and 15 nm diameter in the rat model administered by inhalation. The amount retained in the lungs from 6 h to 7 days was 65% and 40–55%, respectively (Kreyling et al., 2002). Nemmar et al. studied albumin nanocolloid nanoparticles ≤80 nm in size that were intratracheally instilled into hamsters. At their longest time point, 60 min after instillation, 73% of the total radioactivity remained in the lungs (Nemmar et al., 2001). Differences in lung retention for these studies compared to our observations could be due to characteristics of the particles used, including size, surface charge, solubility, or chemical composition. Delivery of particles (inhalation versus instillation) could also account for differences in lung retention. For the mouse model, the work by Furuyama et al. shows retention of 89% for 200-nm gold particles administered by instillation at 2 h (Furuyama et al., 2009). The 200-nm particle retention is similar to our 2-h retention data (93.37% ± 2.67%); but, they did not quantify retention at later time points.

Secondary organ translocation observed in the current studies differed somewhat from the literature. We observed particle transport to the liver only at 24 h (0.10% ± .11%), whereas kidney localization was not observed. In contrast, studies in the literature using slightly smaller particles (~80 nm) saw transport to the liver. Kreyling et al. found 0.0006–0.0008% of the inhaled dose in the liver (at 6 h, 1, 3, 7 days) and 0.001% in the kidneys of rats (Kreyling et al., 2002). Also, Nemmar et al. saw 0.06–1.24% in the liver (at 5, 15, 30, and 60 min after instillation) and noted detectable particles in the kidneys of hamsters but did not give exact amounts (Nemmar et al., 2001). In humans, liver accumulation was not observed for 100-nm particles as reported by Wiebert et al.; however, Nemmar et al. (2002) observed both liver and bladder signal up to 45 min after inhalation. This signal corresponded to 5–25% of the inhaled dose in the bladder (at 5, 10, 20, 30, and 45 min) and 8% of the inhaled dose in the liver over time. Our lack of observation of kidney signal could be due to the concentration of nanoparticles in the tissue. In practice, we required particle concentrations of 1.55×10^{10} nanoparticles/ml to observe detectable signal by PET. GI clearance for our data, either from the swallowing of nanoparticles deposited in the mouth or from the mucociliary escalator, was in agreement with studies in the literature for a variety of particles with different composition and sizes for all three published detection modalities (Kreyling et al., 2002; Semmler et al., 2004; Monleau et al., 2006: Oberdörster et al., 2002; Nemmar et al., 2002).

A frequent concern with the use of radiolabeled particles in tracking studies is whether the radiolabel dissociates from the particles. We therefore performed a number of controls to support that imaging is tracking particles and not dissociated label. First, we compared the biodistribution for free copper versus particles. As shown in Table 2, compared to particles, the majority of the deposited free copper was cleared from the lungs over 48 h (18.52%ID of free copper remains in the lungs versus 93.89%ID of particles), and this loss was statistically significant ($p < .01$). The

Table 3. Literature of PM transport studies in both rodents and humans.

Detection	Particle	Size (nm)	Species	Delivery	% Left in lung	Time	Peripheral organs[#]	Reference
Gamma	^{57}Co oxide	800/1700	Rat	Inhalation	81/95	3 days	Liver, kidneys	Kreyling et al., 1993
					89/96	100 days	GI, skeleton	
					51/91	180 days	Soft tissue	
Gamma	^{192}Iridium	**80**	Rat	Inhalation	65	6 h to 7 days	Liver, kidneys, GI, spleen	Kreyling et al., 2002
		15			40–55	6 h to 7 days	Heart, brain, carcass	
Gamma	^{99m}Tc-albumin	**≤80**	Hamster	Instillation	62	5 min	Liver, heart	Nemmar et al., 2001
					72	15 min	Spleen, kidneys	
					60	30 min	Brain	
					73	60 min		
Gamma	^{192}Iridium	15–20	Rat	Inhalation	82	6 h	Liver, spleen	Semmler et al., 2004
					31	3 weeks	Brain, kidneys	
					17	2 months	GI	
					8	6 months		
ICP-MS	Gold	20/**200**	Mouse	Instillation	75/89	2 h	Heart, liver, spleen, kidney	Furuyama et al., 2009
ICP-MS	UO_4 and UO_2	2540	Rat	Inhalation	100	4 h	GI, kidneys	Monleau et al., 2006
					80	1 day	Femurs	
					40	3 days	Bladder	
					10	8 days		
					<10	16 days		
ICP-MS	^{13}Carbon	20–29	Rat	Inhalation	26–35	0.5 h	Liver	Oberdörster et al., 2002
					33–37	18 h	GI	
					29–36	24 h		
ICP-MS	^{13}Carbon	36	Rat	Inhalation	104	3 days	Olfactory bulb	Oberdörster et al., 2004
					60	5 days	Cerebrum	
					48	7 days	Cerebellum	
ICP-MS	Silver	15	Rat	Inhalation	38	1 day	Lymph nodes	Takenaka et al., 2001
					8	4 days	Nasal cavity	
					4	7 days	Brain, blood	
							Liver, kidney	
	Silver	15	Rat	Instillation	26	1 day	Heart	
					33	4 days		
					27	7 days		
ICP-MS	Gold	16	Rat	Inhalation	100	0 days	Blood	Takenaka et al., 2006
					91	1 day		
					83	4 days		
					78	7 days		
γ-Camera	^{99m}Tc-Carbon	33	Human	Inhalation	85	24 hr	None	Brown et al., 2002
γ-Camera	^{99m}Tc-Carbon	**<100**	Humans	Inhalation	ND	N/A	Liver, bladder,blood, GI	Nemmar et al., 2002
γ-Camera	^{99m}Tc-Carbon	35	Human	Inhalation	102	24 h	Urine, blood	Wiebert et al., 2006b
γ-Camera	^{99m}Tc-Carbon	**100**	Human	Inhalation	99	24 h	None	Wiebert et al., 2006a
					99	46 h		
					99	70 h		
PET	^{64}Cu-PS	100	Mouse	Instillation	94	48 h	GI, Liver,bladder	Results in this paper

Note. ND = not determined; N/A = not applicable.
[#]Extrapulmonary organs detected at all surveyed time points.

average rate of clearance from the lungs was also different for free copper compared to particles (−4.10%DD/h for free copper versus −0.54%DD/h for particles). Lung retention decreased exponentially over time for free copper; this was markedly different from the nanoparticles, which showed no statistical differences in retention over time. The trends for extrapulmonary distribution over the 48 h were also different. For the liver, particles were found at 24 h only in small amounts (0.10%ID ± .11%DD), whereas for free copper accumulation was found at all time points and reached ~5%ID. Bladder signal was present up to 12 h for particles (0.056%ID ± 0.113%DD), whereas for free copper no signal was found in the bladder after the 2-h time point. Finally, stability assays for the particles confirmed that the ^{64}Cu radiolabel remained tightly associated with the particles over the 48-h time period; no significant loss of label was shown over time.

A distinct advantage of PET imaging is that the initial deposition pattern can be visualized in three dimensions and quantified. This is critical for following clearance and transport because the inhalation or instillation methods that are commonly used to deliver nanoparticles to the lungs in studies of transport are not ideal; deposition amount can vary for inhalation, and inhomogeneous deposition in the lungs is common for the instillation method. Previous studies with a variety of inhalation techniques have shown that less than 100% of the administered dose deposits directly into the lungs. For example, a miniaturized nebulization catheter has been shown to deliver only 12% of the applied dose to the lungs (Tronde et al., 2002). Both nasal inhalation and intratracheal nebulization of Pelikan drawing ink A also have been shown to deliver only a fraction of the sample dose to the lungs, 60% and 10%, respectively (Leong et al., 1998). Intratracheal instillation, despite its rapid delivery, does not distribute as evenly as an inhalation technique and can result in a patchy and inhomogeneous lung distribution (Brain et al., 1976). Instillation also can be technically challenging and care must be taken to avoid disturbing the normal breathing pattern or else cough may be induced, which can rapidly clear part of the dose into the mouth and stomach (Tronde et al., 2002). Because initial deposition patterns can vary, data from large number of animals must be averaged together to compensate for variations between animals. Using fewer animals per time point or fewer time points can reduce the number of animals required but neither is desirable as they decrease statistical relevance and pharmacokinetic information. With imaging, the deposition can be determined for individual animals; thus, each animal can serve as its own reference/control and one can directly compare biodistribution data from different time points.

Another unique advantage of PET imaging is that particle movement can be tracked dynamically. Rather than collect a static image at different time points, one can collect a time- lapse series of images to recreate particle movement through the tissue. Dynamic imaging has been used for a variety of applications, including monitoring response of cancer to chemotherapy, evaluation and monitoring of tumor proliferation in glioma-bearing mice, and tracking of progenitor cell therapy for acute myocardial infarction (Bradbury et al., 2008; Doot et al., 2007; Doyle et al., 2007). Dynamic scanning can detect nanoparticle movement on short time scales that could be missed with static acquisition methods.

Although PET provides some excellent advantages to PM transport studies, it does possess some drawbacks. A primary drawback is that the detection limits for PET are lower than for the traditional ex vivo techniques of gamma counting and ICP-MS (Table 1); compared to the detection with gamma counting (3.87×10^9 nanoparticles/ml), PET was 3.3 times less sensitive than gamma counting for the specific activity of particles used in these studies. Thus PET can miss trace amounts of a nanoparticle accumulate in secondary organs. This could be offset somewhat by increasing the amount of radioactivity per particle or using higher activity isotopes. The cost and availability of PET isotopes and imaging facilities can also limit widespread adoption of these methods. The isotopes used for these studies must be purchased commercially unless an on site cyclotron is available; this is not significantly different from the purchase of isotopes used for gamma counting studies, but small animal PET imaging may not be available at all institutions.

Despite these drawbacks, PET can provide additional information and can be advantageous over traditional techniques. Although the gamma camera is capable of providing some initial deposition data, it cannot provide three-dimension information and has low sensitivity, which could limit detection of small amounts of signal in secondary organs. ICP-MS and gamma counting can provide the sensitivity needed for detecting small amounts, but they are not capable of determining the initial lung deposition for each animal and do not give information on particle spatial distribution in organs. Without confirmation of the initial deposition pattern for each animal, it is necessary to harvest organs from a large number of animals at each time point for statistical relevance to compensate for animal-to-animal variation. Multiple animals per time point are also necessary because these techniques analyze organ distribution ex vivo.

These studies verify that nanoparticle deposition and fate of instilled ultrafine particles can be followed using positron emission tomography and that PET can be an advantageous tool for particle transport studies. PET can provide both qualitative and quantitative results and can be applied to image both rat or mouse models. CT or magnetic resonance imaging (MRI) can also be used for anatomical referencing in conjunction with PET. In contrast with traditional gamma counting methods, PET allows visualization and quantitation of initial deposition to the lungs, with the tradeoff of a somewhat weaker sensitivity. PET also allows the researcher to track the biodistribution of particles over time in the *same* animal. Positron emission tomography presents an attractive alternative method that can produce three-dimensional images for tracking particle fate in animal models.

Acknowledgements

We would like to thank the Center for Molecular and Genomic Imaging at UC Davis for their assistance with the animal imaging, and Drs. Kent Pinkerton and Dennis Wilson (University of California at Davis) for helpful discussions. Imaging work performed at the Center for Molecular and Genomic Imaging, University of California, Davis is supported in part by a NCI Small Animal Imaging Resource grant (U24 CA 110804).

Declaration of interest

This research has been funded wholly or in part by the United States Environmental Protection Agency through STAR grant RD832414 to the University of California at Davis. It has not been subjected to the Agency's required peer and policy review and therefore does not necessarily reflect the views of the Agency and no official endorsement should be inferred.

References

Araujo JA, Barajas B, Kleinman M, Wang X, Bennett BJ, Gong KW, Navab M, Harkema J, Sioutas C, Lusis AJ, Nel AE. 2008. Ambient particulate pollutants in the ultrafine range promote early atherosclerosis and systemic oxidative stress. Circ Res 102:589–596.

Bradbury MS, Hambardzumyan D, Zanzonico PB, Schwartz J, Cai S, Burnazi EM, Longo V, Larson SM, Holland EC. 2008. Dynamic small-animal PET imaging of tumor proliferation with 3'-deoxy-3'-^{18}F-fluorothymidine in a genetically engineered mouse model of high-grade gliomas. J Nucl Med 49:422–429.

Brain JD, Knudson DE, Sorokin SP, Davis MA. 1976. Pulmonary distribution of particles given by intra-tracheal instillation or by aerosol inhalation. Environ Res 11:13–33.

Brannon-Peppas L, Blanchette J. 2004. Nanoparticles and targeted systems for cancer therapy. Adv Drug Delivery Rev 56:1649–1659.

Brown JS, Kim CS, Reist PC, Zeman KL, Bennett WD. 2000. Generation of radiolabeled "soot-like" ultrafine aerosols suitable for use in human inhalation studies. Aerosol Sci Technol 32:325–337.

Brown JS, Zeman KL, Bennett WD. 2002. Ultrafine particle deposition and clearance in the healthy and obstructed lung. Am J Respir Crit Care Med 166:1240–1247.

Brunekreef B, Holgate ST. 2002. Air pollution and health. Lancet 360: 1233–1242.

Bushberg JT, Seibert JA, Leidholdt EM, Boone JM. 2002. Radiation detection and measurement and nuclear imaging. In: The Essential Physics of Medical Imaging. 2nd ed. Philadelphia, PA: Lippincott Williams and Wilkins, 656–657, 683.

Cherry SR. 2001. Fundamentals of positron emission tomography and applications in preclinical drug development. J Clin Pharmacol 41:482–491.

Cherry SR, Sorenson JA, Phelps ME. 2003. Counting systems and the gamma camera: Performance characteristics. In: Physics in Nuclear Medicine. 3rd ed. Philadelphia, PA: Saunders, 185–187, 247-251.

Ding H, Goldberg MM, Raymer JH, Holmes J, Stanko J, Chaney SG. 1999. Determination of platinum in rat dorsal root ganglion using ICP-MS. Biol Trace Element Res 67:1–11.

Dockery DW, Pope CA, Xu X, Spengler JD, Ware JH, Fay ME, Ferris BG, Speizer FE. 1993. An association between air pollution and mortality in six U.S. cities. N Engl J Med 329:1753–1759.

Dominici F, McDermott A, Zeger SL, Samet JM. 2003. National maps of the effects of particulate matter on mortality: Exploring geographical variation. Environ Health Perspect 111:39–43.

Donaldson K, Stone V, Gilmour PS, Brown DM, MacNee W. 2000. Ultrafine particles: Mechanisms of lung injury. Phil Trans R Soc Lond A 358:2741–2749.

Doot RK, Dunnwald LK, Schubert EK, Muzi M, Peterson LM, Kinahan PE, Kurland BF, Mankoff D.A. 2007. Dynamic and static approaches to quantifying ^{18}F-FDG uptake for measuring cancer response to therapy, including the effect of granulocyte CSF. J Nucl Med 48:920–925.

Doyle B, Kemp BJ, Chareonthaitawee P, Reed C, Schmeckpeper J, Sorajja P, Russell S, Araoz P, Riederer SJ, Caplice NM. 2007. Dynamic tracking during intracoronary injection of ^{18}F-FDG-labeled progenitor cell therapy for acute myocardial infarction. J Nucl Med 48:1708–1714.

Ferin J, Oberdorster G, Penney DP. 1992. Pulmonary retention of ultrafine and fine particles in rats. Am J Respir Cell Mol Biol 6:535–542.

Foster MW, Walters DM, Longphre M, Macri K, Miller LM. 2001. Methodology for the measurement of mucociliary function in the mouse by scintigraphy. J Appl Physiol 90:1111–1118.

Franc BL, Acton PD, Mari C, Hasegawa BH. 2008. Small-animal SPECT and SPECT/CT: Important tools for preclinical investigation. J Nucl Med 49:1651–1663.

Furuyama A, Kanno S, Kobayashi T, Hirano S. 2009. Extrapulmonary translocation of intratracheally instilled fine and ultrafine particles via direct and alveolar macrophage-associated routes. Arch Toxicol 83: 429–437.

Gerlofs-Nijland ME, Boere AJF, Leseman DLAC, Dormans JAMA, Sandström, Salonen RO, van Bree L, Cassee FR. 2005. Effects of particulate matter on the pulmonary and vascular system: Time course in spontaneously hypertensive rats. Part Fibre Toxicol 2:2.

Goertzen AL, Young Suk J, Thompson CJ. 2007. Imaging of weak-source distributions in LSO-based small-animal PET scanners. J Nucl Med 48:1692–1698.

Jarrett BR, Gustafsson B, Kukis DL, Louie AY. 2008. Synthesis of ^{64}Cu-labeled magnetic nanoparticles for multimodal imaging. Bioconjugate Chem 197:1496–1504.

Kim JS, Lee JS, Im KC, Kim SJ, Kim SY, Lee DS, Moon DH. 2007. Performance measurement of the microPET Focus 120 scanner. J Nucl Med. 48:1527–1535.

Kiryu S, Sundaram T, Kubo S, Ohtomo K, Asakura T, Gee JC, Hatabu H, Takahashi M. 2008. MRI assessment of lung parenchymal motion in normal mice and transgenic mice with sickle cell disease. J Magn Res Imag 27:49–56.

Kreyling WG, Cox C, Ferron GA, Oberdörster G. 1993. Lung clearance in longsevans rats after inhalation of porous, monodisperse cobalt oxide particles. Exp Lung Res 19:445–467.

Kreyling WG, Semmler M, Erbe F, Mayer P, Takenaka S, Shultz H. 2002. Translocation of ultrafine insoluble iridium particles from lung epithelium to extrapulmonary organs is size dependent but very low. J Toxicol Environ Health A 65:1513–1530.

Laden F, Neas LM, Dockery DW, Schwartz J. 2000. Association of fine particulate matter from different sources with daily mortality in six US cities. Environ Health Perspect 108:941–947.

Laden F, Schwartz J, Speizer FE, Dockery DW. 2006. Reduction in fine particulate air pollution and mortality: Extended follow-up of the Harvard six cities study. Am J Respir Crit Care Med 173:667–672.

Leong BK, Coombs JK, Sabaitis CP, Rop DA, Aaron CS. 1998. Quantitative morphometric analysis of pulmonary deposition of aerosol particles inhaled via intratracheal nebulization, intratracheal instillation or nose-only inhalation. J Appl Toxicol 18:149–160.

Li XY, Brown D, Smith S, MacNee W, Donaldson K. 1999. Short-term inflammatory responses following intratracheal instillation of fine and ultrafine carbon black in rats. Inhal Toxicol 11:709–731.

Loudos GK, Nikita KS, Giokaris ND, Styliaris E, Archimandritis SC, Varvarigou AD, Papanicolas CN, Majewski S, Weisenberger D, Pani R, Scopinaro F, Uzunoglu NK, Maintas D, Stefanis K. 2003. A 3D high-resolution gamma camera for radiopharmaceutical studies with small animals. Appl Radiat Isot 58:501–508.

McClellan RO, Henderson RF. 1989. Deposition and clearance of inhaled particles. In: Concepts in Inhalation Toxicology. 2nd ed. Washington, DC: Taylor and Francis, 203–209.

Monleau M, De Méo M, Frelon S, Paquet F, Donnadieu-Claraz M, Duménil G, Chazel V. 2006. Distribution and genotoxic effects after successive exposure to different uranium oxide particles inhaled by rats. Inhal Toxicol 18:885–894.

Moi MK, Meares CF, McCall MJ, Cole WC, DeNardo SJ. 1985. Copper chelates as probes of biological systems: Stable copper complexes with a macrocyclic bifunctional chelating agent. Anal Biochem 148:249–253.

Nemmar A, Vanbilloen H, Hoylaerts MF, Hoet PHM, Verbruggen A, Nemery B. 2001. Passage of intratracheally instilled ultrafine particles from the lung into systemic circulation in hamsters. Am J Respir Crit Care Med 164:1665–1668.

Nemmar A, Hoet PHM, Vanquickenborne B, Dinsdale D, Thomeer M, Hoylaerts MF, Vanbilloen H, Mortelmans L, Nemery B. 2002. Passage of inhaled particles into the blood circulation in humans. Circulation 105:411–414.

Oberdörster G, Ferin J, Finkelstein G, Wade P, Corson N. 1990. Increased pulmonary toxicity of ultrafine particles 2. Lung lavage studies. J Aerosol Sci 21:384–387.

Oberdörster G, Ferin J, Soderholm S, Gelein R, Cox C, Baggs R, Morrow PE. 1994. Increased pulmonary toxicity of inhaled ultrafine particles: Due to lung overload alone? Ann Occup Hyg 38:295–302.

Oberdörster G, Sharp Z, Atudorei V, Elder A, Gelein R, Lunts A, Kreyling W, Cox C. 2002. Extrapulmonary translocation of ultrafine particles following whole-body inhalation exposure of rats. J Toxicol Environ Health A 65:1531–1543.

Oberdörster G, Sharp Z, Atudorei V, Elder A, Gelein R, Kreyling W, Cox C. 2004. Translocation of inhaled ultrafine particles to the brain. Inhal Toxicol 16:437–445.

Ostro BD. 1990. Associations between morbidity and alternative measures of particulate matter. Risk Anal 10:421–427.

Peters A, Dockery D, Heinrich J, Wichmann H. 1997. Short-term effects of particulate air pollution on respiratory morbidity in asthmatic children. Eur Respir J. 10:872–879.

Peters A, Dockery DW, Muller JE, Mittleman MA. 2001. Increased particulate air pollution and the triggering of myocardial infarction. Circulation 103:2810–2815.

Peters A, von Klot S, Heier M, Trentinaglia I, Hormann A, Wichmann HE, Lowel H. 2004. Exposure to traffic and the onset of myocardial infarction. N Engl J Med 351:1721–1730.

Riediker M, Cascio WE, Griggs TR, Herbst MC, Bromberg PA, Neas L, Williams RW, Devlin RB. 2004. Particulate matter exposure in cars is associated with cardiovascular effects in healthy young men. Am J Respir Crit Care Med 169:934–940.

Reich BJ, Fuentes M, Burke J. 2009. Analysis of the effects of ultrafine particulate matter while accounting for human exposure. Environmetrics 20:131–146.

Rossin R, Muro S, Welch MJ, Muzykantov VR, Schuster DP. 2008. In vivo imaging of ^{64}Cu-labeled polymer nanoparticles targeted to the lung endothelium. J Nucl Med 49:103–111.

Saldiva PHN, Pope CA, Schwartz J, Dockery DW, Lichtenfels AJ, Salge JM, Barone I, Bohm GM. 1995. Air-pollution and mortality in elderly people—A time-series study in Sao Paulo, Brazil. Arch Environ Health 50: 159–163.

Schwartz J, Morris R. 1995. Air pollution and hospital admissions for cardiovascular disease in Detroit, Michigan. Am J Epidemiol 42:23–35.

Semmler M, Seitz J, Erbe F, Mayer P, Heyder J. 2004. Long-term clearance kinetics of inhaled ultrafine insoluble iridium particles from the rat lung, including transient translocation into secondary organs. Inhal Toxicol 16:453–459.

Stölzel M, Breitner S, Cyrys J, Pitz M, Wolke G, Kreyling W, Heinrich J, Wichmann H-E, Peters A. 2007. Daily mortality and particulate matter in different size classes in Erfurt, Germany. J Expo Sci Environ Epidemiol 17:458–467.

Takenaka S, Karg E, Roth C, Schulz H, Ziesenis A, Heinzmann U, Schramel P, Heyder J. 2001. Pulmonary and systemic distribution of inhaled ultrafine silver particles in rats. Environ Health Perspect 109(Suppl 4):547–551.

Takenaka S, Karg E, Kreyling W.G, Lentner B, Möller W, Behnke-Semmler M, Jennen L, Walch A, Michalke B, Schramel P, Heyder J, Schulz H. 2006. Distribution pattern of inhaled ultrafine gold particles in the rat lung. Inhal Toxicol 18:733–740.

Tai YC, Chatziioannou AF, Yang Y, Silverman RW, Meadors K, Siegel S, Newport DF, Stickel JR, Cherry SR. 2003. MicroPET II: Design, development and initial performance of an improved microPET scanner for small-animal imaging. Phys Med Biol 48:1519–1537.

Tronde A, Baran G, Eirefelt S, Lennernas H, Bengtsson UH. 2002. Miniaturized nebulization catheters: A new approach for delivery of defined aerosol doses to the rat lung. J Aerosol Med 15:283–296.

US EPA. 2004. Air Quality Criteria for Particulate Matter. Washington, DC: US Environmental Protection Agency. EPA 600/P-99/002aF-bF.

Wichers LB, Nolan JP, Winsett DW, Ledbetter AD, Kodavanti UP, Schladweiler MCJ, Costa DL, Watkinson WP. 2004. Effects of instilled combustion-derived particles in spontaneously hypertensive rats. Part I: Cardiovascular responses. Inhal Toxicol 16:391–405.

Wiebert P, Sanchez-Crespo A, Seitz J, Falk R, Philipson K, Kreyling WG, Möller W, Sommerer K, Larsson S, Svartengren M. 2006a. Negligible clearance of ultrafine particles retained in healthy and affected human lungs. Eur Respir J 28:286–290.

Wiebert P, Sanchez-Crespo A, Falk R, Philipson K, Lundin A, Larsson S, Möller W, Kreyling WG, Svartengren M. 2006b. No Significant translocation of inhaled 35-nm carbon particles to the circulation in humans. Inhal Toxicol 18:741–747.

Wilson MA. 1998. Emission tomography. In: Textbook of Nuclear Medicine. Philadelphia, PA: Lippincott-Raven Publishers, 455–456, 459–461.

Wolff RK, Henderson RF, Snipes MB, Griffith WC, Mauderly JL, Cuddihy RG, McClellan RO. 1987. Alterations of particle accumulation and clearance in lungs of rats chronically exposed to diesel exhaust. Fundam Appl Toxicol 9:154–166.

Xu JY, Li QN, Li JG, Ran TC, Wu SW, Song WM, Chen SL, Li WX. 2007. Biodistribution of ^{99m}Tc-$C_{60}OH_x$ in Sprague-Dawley rats after intratracheal instillation. Carbon 45:1865–1870.

Yang YF, Rendig S, Siegel S, Newport DF, Cherry SR. 2005. Cardiac PET imaging in mice with simultaneous cardiac and respiratory gating. Phys Med Biol 50:2979–2989.

Yu LE, Lanry Yung LY, Ong CN, Tan YL, Suresh Balasubramaniam K, Hartono D, Shui G, Wenk MR, Ong WY. 2007. Translocation and effects of gold nanoparticles after inhalation exposure in rats. Nanotoxicology 1:235–242.